

Journal of Mechanics of Materials and Structures

**ELECTROTHERMOMECHANICAL BEHAVIOR OF A RADIALY POLARIZED
ROTATING FUNCTIONALLY GRADED PIEZOELECTRIC CYLINDER**

Ali Ghorbanpour Arani, Abbas Loghman, Ali Abdollahitaheri and Vahid Atabakhshian

Volume 6, No. 6

July–August 2011

ELECTROTHERMOMECHANICAL BEHAVIOR OF A RADially POLARIZED ROTATING FUNCTIONALLY GRADED PIEZOELECTRIC CYLINDER

ALI GHORBANPOUR ARANI, ABBAS LOGHMAN,
ALI ABDOLLAHITAHERI AND VAHID ATABAKHSHIAN

A hollow circular cylinder made of exponentially graded piezoelectric material, such as PZT_4, is considered. Loading is composed of internal and external pressures, a distributed temperature field due to steady state heat conduction with convective boundary condition, an inertia body force due to rotation with constant angular velocity and a constant electric potential difference between its inner and outer surfaces. The material properties except Poisson's ratio and thermal conduction coefficient are assumed to be exponentially distributed along radius. The governing equation in polarized form is shown to reduce to a second-order ordinary differential equation with variable coefficients for the radial displacement. In this article, a closed form solution is presented for this ODE by employing hypergeometric functions such as Whittaker's M and W functions. Also we have considered four different sets of boundary conditions. The electrothermomechanical induced stresses and the electric potential distributions are investigated for the piezoceramic PZT_4 cylinder. It is concluded that the inhomogeneity exponent μ plays a substantial role in radial and circumferential stress distributions. Therefore, the results of this investigation can contribute to the design of EGPM rotating thick-walled circular cylinders.

A list of symbols can be found on page 881.

1. Introduction

In recent years there has been a resurgence of interest in piezoelectricity, due to advances in the intelligent structures technology. It is well known that piezoelectric materials experience mechanical deformations when placed in an electric field, and become electrically polarized under mechanical loads and in fact they exhibit electromechanical coupling. Piezoelectric materials have been used for a long time to make many electromechanical devices. One of the first applications of the piezoelectric effect was an ultrasonic submarine detector developed during the First World War. Other applications include transducers for converting electrical energy to mechanical energy or vice versa, resonators and filters for frequency control and selection for telecommunication and precise timing and synchronization, and acoustic wave sensors. To amend the structure of piezoelectric material and the application of these materials in various environments, functionally graded piezoelectric materials (FGPM) have been created. The mechanical and thermal properties of FGPM are similar to FGM, varying continuously in terms of the spatial coordinate system.

For homogeneous piezoelectric media, Ghorbanpour et al. [2006] investigated the stress distribution of dielectric potential fields in piezoelectric hollow spheres. Their results showed that an existing mechanical hoop stress distribution can be neutralized by a suitably applied electric field. Saadatfar and Razavi

Keywords: EGPM, rotating cylinder, hypergeometric function, electrothermomechanical stress, electric potential.

[2009] analyzed the stress in piezoelectric hollow cylinder with thermal gradient. An analytic solution to the axisymmetric problem of an infinitely long, radially polarized, radially orthotropic piezoelectric hollow circular cylinder was developed in [Galic and Horgan 2002].

For a special inhomogeneous case, Lu et al. [2005] derived the exact three-dimensional analytical solutions for a rectangular laminate with piezoelectric layers of exponentially graded material properties along thickness, and under simply supported boundary conditions along two opposite edges. They discussed some properties of the mechanical and electric responses of the FGPM plates under mechanical and/or electrical forces, and they also showed the influence of material gradients by numerical examples based on the exact solutions.

Zhong and Shang [2003] presented an exact solution of a simply supported functionally gradient piezoelectric rectangular plate based on three-dimensional electroelasticity theory. The obtained exact solution was valid for arbitrary mechanical and electric loads applied on the upper and lower surfaces of the plate and could serve as a benchmark result to assess other approximate methodologies or as a basis for establishing simplified FGPM plate theories.

The three-dimensional exact solutions of a simply supported FGPM plate/laminate were obtained based on an alternative approach in [Lu et al. 2006], which compared the exact solutions with the solutions obtained in [Zhong and Shang 2003], and concluded that their exact solutions may be more convenient for further treatments of both analytical and numerical studies.

Pan and Han [2005] also presented an exact solution for a multilayered rectangular plate made of anisotropic and functionally graded magneto-electroelastic materials. The plate is simply supported along its edges, and both mechanical and electric loads are applied on the top surface. Their numerical results showed the influence of the exponential factor, magneto-electroelastic properties, stacking sequence and loading types on the induced magneto-electroelastic fields, which should be of interest to the design of smart structures.

The static analysis of a single-layered functionally graded piezoelectric plate, in both sensor and actuator configuration was investigated in [Brischetto and Carrera 2009], which compared refined theories with classical ones, to demonstrate the effectiveness of these theories in the case of FGPMs.

Recently, Li et al. [2010] analyzed an axisymmetric electroelastic problem of hollow radially polarized piezoceramic cylinders made of FGMs as sensors and actuators. For two typical cases of sensors and actuators, the response of the radial and circumferential stresses as well as the electric potential was shown graphically by them. Their derived results for the distribution of hoop and radial stresses as well as the electric response are useful in designing hollow cylindrical FG piezoelectric sensors/ actuators.

The elastic and piezoelectric properties vary as a power-function along radius, Khoshgoftar et al. [2009] studied thermopiezoelectric behavior of a thick-walled cylinder made of FGMs subjected to a temperature gradient and inner and outer pressures.

Babaei and Chen [2008] presented the analytical solution for a radially piezoelectric functionally graded rotating hollow shaft. The analytical solution of a functionally graded piezothermoelastic hollow cylinder was presented in [Chen and Shi 2005]. This article assumed that only the piezoelectric coefficient was varying quadratically in the radial direction while the other material parameters were assumed to be constants. They neglected other inhomogeneity parameters such as thermal conduction coefficient and modulus of elasticity. Because of this incompleteness and more accordance of exponential form of

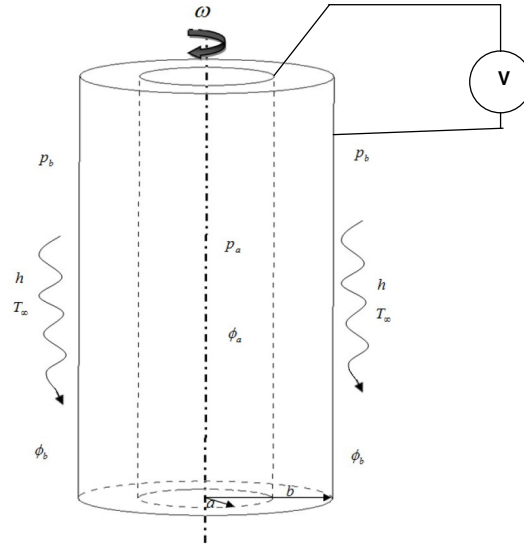


Figure 1. Configuration of an EGPM rotating hollow circular cylinder.

properties with new practical model, the effect of the entire material inhomogeneity on the piezothermo-electroelastic behavior of an EGPM hollow rotating cylinder is studied in the present paper.

In this study a thick-walled rotating cylinder of radially polarized anisotropic piezoelectric material, such as PZT_4, is assumed. The cylinder is subjected to mechanical and thermal loads, together with a potential difference induced by electrodes attached to the inner and outer surfaces (Figure 1). All the mechanical, thermal and piezoelectric properties of the EGPM rotating hollow cylinder, except Poisson's ratio, are assumed to be radial dependent and they are expressed as exponential functions of r . The governing equations of exponentially graded piezoelectric cylindrical structure in radially polarized form are reduced to a second-order inhomogeneous differential equation in terms of displacement with variable coefficients and is solved using hypergeometric functions and Simpson's integrating method. Finally, numerical results and the associated data are presented for four different sets of boundary conditions to illustrate electroelastic stresses, electric potential, radial displacement and thermal distributions for piezoceramic, PZT_4.

2. Heat conduction problem

In this section, the axisymmetric, steady state, heat conduction equation in the cylindrical coordinate system with the thermal boundary condition is given as (see [Hosseini et al. 2007])

$$\begin{aligned} \frac{1}{r} \frac{\partial}{\partial r} \left[rk(r) \frac{\partial T(r)}{\partial r} \right] &= 0, \quad (a \leq r \leq b), \\ T(r)|_{r=a} &= T_0, \\ \left[\frac{\partial T(r)}{\partial r} + hT(r) \right] \Big|_{r=b} &= 0, \end{aligned} \quad (1)$$

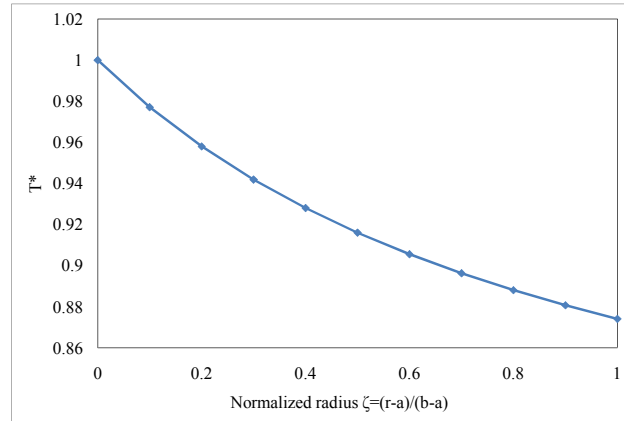


Figure 2. Temperature distribution versus normalized radius for $\beta = 1$.

where h is the ratio of convective heat transfer coefficient and $k(r)$ is the thermal conduction coefficient, which is assumed to be a power function of r as

$$k(r) = k_0 r^\beta, \tag{2}$$

Substituting (2) into the heat conduction equation (1) one can obtain

$$\frac{1}{r} \frac{\partial}{\partial r} \left[r^{\beta+1} \frac{\partial T(r)}{\partial r} \right] = 0, \tag{3}$$

the general solution for the temperature distribution is obtained by integrating (3), as

$$T(r) = D_1 r^{-\beta} + D_2, \tag{4}$$

where D_1 and D_2 are obtained from the thermal boundary conditions as follows:

$$D_1 = \frac{hT_0}{\beta b^{-(\beta+1)} + h(a^{-\beta} - b^{-\beta})}, \quad D_2 = \frac{T_0[\beta b^{-(\beta+1)} - hb^{-\beta}]}{\beta b^{-(\beta+1)} + h(a^{-\beta} - b^{-\beta})}. \tag{5}$$

The temperature distribution thus obtained is illustrated in Figure 2.

3. Basic formulation

In this section, the general differential equation of a rotating hollow cylinder with inhomogeneous material properties is obtained. The material properties are exponentially variable along the radial direction as follows:

$$\begin{aligned} c_{ij}(r) &= c_{ij0} \exp\left(\mu \frac{r-a}{b-a}\right), & e_{1i}(r) &= e_{1i0} \exp\left(\mu \frac{r-a}{b-a}\right), & g_{11}(r) &= g_{110} \exp\left(\mu \frac{r-a}{b-a}\right), \\ p_{11}(r) &= p_{110} \exp\left(\mu \frac{r-a}{b-a}\right), & \rho(r) &= \rho_0 \exp\left(\mu \frac{r-a}{b-a}\right), \end{aligned} \tag{6}$$

where c_{ij} ($i, j = 1, 2$), e_{1i} ($i = 1, 2$), g_{11} , p_{11} and $\rho(r)$ are elastic constants, piezoelectric constants, dielectric constant, pyroelectric coefficient and mass density, respectively. The constants c_{ij0} , e_{1i0} , g_{110} , p_{110} and ρ_0 are the material properties of the inner surface, while μ is the material inhomogeneity parameter.

In this study, we can assume the cylinder is long enough to guarantee a plane strain condition.

Thus, for this case all the field variables are the function of radial coordinate r and circumferential displacement u_θ is zero as

$$u_r = u_r(r), \quad u_z = 0, \quad u_\theta = 0, \quad \phi = \phi(r), \quad (7a)$$

where ϕ is the electric potential.

The radial and circumferential strains and the relation between electric field and electric potential are written as

$$\varepsilon_r = \frac{\partial u}{\partial r}, \quad \varepsilon_\theta = \frac{u}{r}, \quad E_r = -\frac{\partial \phi(r)}{\partial r}. \quad (7b)$$

The constitutive relations of stresses and displacement in radially polarized piezoelectric cylinder and the component of radial electric displacement vector are written as (see [Dai et al. 2010])

$$\sigma_r = c_{11} \frac{\partial u}{\partial r} + c_{12} \frac{u}{r} + e_{11} \frac{\partial \phi(r)}{\partial r} - \lambda_1 T(r), \quad (8a)$$

$$\sigma_\theta = c_{12} \frac{\partial u}{\partial r} + c_{22} \frac{u}{r} + e_{12} \frac{\partial \phi(r)}{\partial r} - \lambda_2 T(r), \quad (8b)$$

$$D_r = e_{11} \frac{\partial u}{\partial r} + e_{12} \frac{u}{r} + g_{11} \frac{\partial \phi(r)}{\partial r} + p_{11} T(r), \quad (8c)$$

where σ_r, σ_θ are radial and circumferential stresses, D_r is the radial electric displacement and the thermal modulus λ_1, λ_2 are given by

$$\lambda_1 = c_{11}\alpha_1 + c_{12}\alpha_2, \quad \lambda_2 = c_{12}\alpha_1 + c_{22}\alpha_2. \quad (9)$$

The equation of equilibrium and the charge equation of rotating cylinder are expressed as (see [Tiersten 1969; Fung 1965])

$$\frac{\partial \sigma_r}{\partial r} + \frac{\sigma_r - \sigma_\theta}{r} + \rho r \omega^2 = 0, \quad (10a)$$

$$\frac{\partial D_r}{\partial r} + \frac{D_r}{r} = 0. \quad (10b)$$

4. Solution procedure

By solving the differential equation (10b) the electrical displacement is obtained as

$$D_r(r) = \frac{A_1}{r}, \quad (11)$$

Substituting (11) into (8c) the following equation is obtained for potential gradient as

$$\frac{\partial \phi(r)}{\partial r} = \frac{1}{g_{110}} \left[e_{110} \frac{\partial u}{\partial r} + e_{120} \frac{u}{r} + p_{110} T(r) - \frac{A_1}{r} \exp\left(-\mu \frac{r-a}{b-a}\right) \right], \quad (12)$$

where A_1 is a constant.

Substituting (12) into (8a) and (8b), the radial and hoop stresses can be rewritten as

$$\begin{aligned} \sigma_r &= e^{\xi(r-a)} \left[w_1 \frac{\partial u}{\partial r} + w_2 \frac{u}{r} + w_3 T(r) \right] - \frac{w_4 A_1}{r}, \\ \sigma_\theta &= e^{\xi(r-a)} \left[w_2 \frac{\partial u}{\partial r} + w_5 \frac{u}{r} + w_6 T(r) \right] - \frac{w_7 A_1}{r}. \end{aligned} \tag{13}$$

Substituting (13) into (10a) the governing differential equation for the problem in terms of radial displacement u and temperature distribution $T(r)$ is derived as

$$\begin{aligned} r^2 \frac{\partial^2 u}{\partial r^2} + (1 + \xi r)r \frac{\partial u}{\partial r} + \frac{\xi w_2 r - w_5}{w_1} u \\ = - \frac{\xi w_3 r^2 + r(w_3 - w_6)}{w_1} T(r) - \frac{w_3}{w_1} r^2 \frac{\partial T(r)}{\partial r} - \frac{\rho_0 \omega^2}{w_1} r^3 - \frac{w_7 A_1}{w_1} e^{-\xi(r-a)}, \end{aligned} \tag{14}$$

where

$$\begin{aligned} w_1 &= c_{110} + \frac{e_{110}^2}{g_{110}}, & w_2 &= c_{120} + \frac{e_{110} e_{120}}{g_{110}}, & w_3 &= \frac{e_{110}}{g_{110}} - c_{110} \alpha_{10} - c_{120} \alpha_{20}, \\ w_4 &= \frac{e_{110}}{g_{110}}, & w_5 &= c_{220} + \frac{e_{120}^2}{g_{110}}, & w_6 &= \frac{e_{120} p_{110}}{g_{110}} - c_{120} \alpha_{10} - c_{220} \alpha_{20}, \\ w_7 &= \frac{e_{120}}{g_{110}}, & \xi &= \frac{\mu}{b-a}. \end{aligned} \tag{15}$$

Substituting the temperature distribution (4) into (14) yields

$$r^2 \frac{\partial^2 u}{\partial r^2} + (1 + \xi r)r \frac{\partial u}{\partial r} + \frac{\xi w_2 r - w_5}{w_1} u = F(r). \tag{16}$$

The inhomogeneous term on the right-hand-side of (16) is denoted by $F(r)$ as follows

$$F(r) = -D_2 \frac{\xi w_3 r^2 + r(w_3 - w_6)}{w_1} - D_1 \frac{\xi w_3 r + w_3 - w_6 - w_3 \beta}{w_1} r^{1-\beta} - \frac{\sigma_0 \omega^2}{w_1} r^3 - \frac{w_7 A_1}{w_1} e^{-\xi(r-a)}. \tag{17}$$

The general solution of (16) is assumed to be in the form

$$u(r) = C_1 P(r) + C_2 Q(r) + R(r), \tag{18}$$

where C_1 and C_2 are arbitrary integration constants, $P(r)$ and $Q(r)$ are homogenous solutions, and $R(r)$ is the particular solution.

A particular solution can be developed by employing the variation of parameter method:

$$R(r) = -P(r) \int_a^r \frac{Q(r)F(r)}{W(r)} dr + Q(r) \int_a^r \frac{P(r)F(r)}{W(r)} dr. \tag{19}$$

where $W(r)$ is the Wronskian of $P(r)$, $Q(r)$, defined by

$$W(r) = P(r) \frac{dQ}{dr} + Q(r) \frac{dP}{dr}. \tag{20}$$

The homogeneous solution of the corresponding differential equation (16) is obtained using Maple as

$$P(r) = \frac{e^{-\xi r/2} {}^W W\left(\frac{2w_2-w_1}{2w_1}, \sqrt{\frac{w_5}{w_1}}, \xi r\right)}{\sqrt{r}}, \quad Q(r) = \frac{e^{-\xi r/2} {}^W M\left(\frac{2w_2-w_1}{2w_1}, \sqrt{\frac{w_5}{w_1}}, \xi r\right)}{\sqrt{r}}, \quad (21)$$

where the Whittaker functions ${}^W M$ and ${}^W W$ are defined in the sidebar below (for details see [Abramowitz and Stegun 1965] or [Brischetto and Carrera 2009], for instance). A particular solution is obtained by the method of variation of parameters; defining

$$\Delta = -(D_1 r^{1-\beta} \xi w_3 - ((\beta - 1)w_3 + w_6)D_1 r^{-\beta} + D_2(1 + \xi r)w_3 - w_6 D_2 + \rho_0 r^2 \omega^2) e^{\xi r/2},$$

we can write

$$R(r) = \frac{e^{-\xi r/2}}{\sqrt{r}} \left[\begin{aligned} & {}^W M\left(\frac{2w_2-w_1}{2w_1}, \sqrt{\frac{w_5}{w_1}}, \xi r\right) \int_a^r {}^W W\left(\frac{2w_2-w_1}{2w_1}, \sqrt{\frac{w_5}{w_1}}, \xi r\right) \sqrt{r} \Delta \frac{dr}{W(r)} \\ & - {}^W W\left(\frac{2w_2-w_1}{2w_1}, \sqrt{\frac{w_5}{w_1}}, \xi r\right) \int_a^r {}^W M\left(\frac{2w_2-w_1}{2w_1}, \sqrt{\frac{w_5}{w_1}}, \xi r\right) \sqrt{r} \Delta \frac{dr}{W(r)} \\ & + w_7 A_1 {}^W M\left(\frac{2w_2-w_1}{2w_1}, \sqrt{\frac{w_5}{w_1}}, \xi r\right) \int_a^r {}^W W\left(\frac{2w_2-w_1}{2w_1}, \sqrt{\frac{w_5}{w_1}}, \xi r\right) \frac{e^{\xi(a-r/2)}}{\sqrt{r} W(r)} dr \\ & - w_7 A_1 {}^W W\left(\frac{2w_2-w_1}{2w_1}, \sqrt{\frac{w_5}{w_1}}, \xi r\right) \int_a^r {}^W M\left(\frac{2w_2-w_1}{2w_1}, \sqrt{\frac{w_5}{w_1}}, \xi r\right) \frac{e^{\xi(a-r/2)}}{\sqrt{r} W(r)} dr \end{aligned} \right].$$

Substituting (18) into (12) and integrating, the electric potential $\phi(r)$ is obtained:

$$\phi(r) = \frac{1}{g_{110}} \left[e_{110} u(r) + e_{120} \int_a^r \frac{u(r)}{r} + p_{110} T(r) - \int_a^r \frac{A_1}{r} \exp\left(-\mu \frac{r-a}{b-a}\right) \right] + A_2. \quad (22)$$

The Whittaker functions ${}^W M$ and ${}^W W$ are defined by

$$\begin{aligned} {}^W M(k, u, z) &= e^{-z/2} z^{u+\frac{1}{2}} {}^K M\left(u-k+\frac{1}{2}, 1+2y; z\right), \\ {}^W W(k, u, z) &= e^{-z/2} z^{u+\frac{1}{2}} {}^K U\left(u-k+\frac{1}{2}, 1+2y; z\right), \end{aligned} \quad (23)$$

where ${}^K M$ and ${}^K U$, known as Kummer functions, are certain generalized hypergeometric series. With the notation $(\alpha)_n = \alpha(\alpha+1)(\alpha+2)\dots(\alpha+n-1)$, we have

$$\begin{aligned} {}^K M(\alpha, \beta, z) &= \sum_{n=0}^{\infty} \frac{(\alpha)_n z^n}{(\beta)_n n!}, \\ {}^K U(\alpha, \beta, z) &= \frac{\Gamma(1-\beta)}{\Gamma(\alpha-\beta+1)} {}^K M(\alpha, \beta, z) + \frac{\Gamma(\beta-1)}{\Gamma(\alpha)} z^{1-\beta} {}^K M(\alpha-\beta+1, 2-\beta, z), \end{aligned} \quad (24)$$

where Γ denotes the usual gamma function.

Substituting the general solution (18) into (13), the radial and circumferential stresses are obtained as

$$\sigma_r(r) = e^{\xi(r-a)} \left[w_1 \frac{\partial u(r)}{\partial r} + w_2 \frac{u(r)}{r} + w_3 T(r) \right] - \frac{w_4 A_1}{r}, \tag{25}$$

$$\sigma_\theta(r) = e^{\xi(r-a)} \left[w_2 \frac{\partial u(r)}{\partial r} + w_5 \frac{u(r)}{r} + w_6 T(r) \right] - \frac{w_7 A_1}{r}, \tag{26}$$

where σ_r , σ_θ and ϕ are radial stress, hoop stress and electric potential, respectively.

Four unknown constants A_1 , C_1 , C_2 and A_2 are determined by the boundary conditions as

$$\sigma_r(a) = -P_a, \quad \sigma_r(b) = -P_b, \quad \phi(a) = \phi_a, \quad \phi(b) = \phi_b. \tag{27}$$

5. Numerical results and discussion

In this section, numerical results are presented graphically for Electric displacement, electrothermoelastic stresses and electric potential of the EGPM rotating hollow cylinder in four cases of boundary conditions as follows:

$$\text{Case 1: } \sigma_r(a) = -P_a, \quad \sigma_r(b) = 0, \quad \phi(a) = 0, \quad \phi(b) = 0. \tag{28}$$

$$\text{Case 2: } \sigma_r(a) = 0, \quad \sigma_r(b) = 0, \quad \phi(a) = \phi_a, \quad \phi(b) = 0. \tag{29}$$

$$\text{Case 3: } \sigma_r(a) = 0, \quad \sigma_r(b) = -P_b, \quad \phi(a) = 0, \quad \phi(b) = 0. \tag{30}$$

$$\text{Case 4: } \sigma_r(a) = -P_a, \quad \sigma_r(b) = -P_b, \quad \phi(a) = \phi_a, \quad \phi(b) = 0. \tag{31}$$

The cylinders are assumed to be made of PZT_4, whose properties are listed in the Table 1.

For all cases, the following data for geometry, material properties, boundary and loading conditions are considered: $a = 0.1$ m, $b = 0.2$ m, $\omega = 400$ rad/s, $P_a = 3 \cdot 10^7$ (Pa), $\phi_a = 1000$ (W/A), $T_0 = 20^\circ\text{C}$, $\beta = 1$, $\mu = -2, -1, 0, 1, 2$.

The results are reported based on the normalized variables

$$\zeta = \frac{r-a}{b-a}, \quad \sigma_i^* = \frac{\sigma_i}{P_a} \quad (i = r, \theta), \quad U^* = \frac{u(r)}{a}, \quad \Phi^* = \frac{\phi}{\phi_a}, \quad T^* = \frac{T(r)}{T_0}. \tag{32}$$

Case 1. In Figure 3 results are shown for case 1, where internal pressure is applied. Figure 3, top left, depicts the distribution of radial stress along the radius for different values of μ . It is seen from the figure that the radial stresses satisfy the mechanical boundary conditions. The distributions of the hoop stresses for different values of μ are displayed in Figure 3, top right. In this figures we can easily observe a reference stress point at $\zeta = 0.2$ in which the hoop stress is identical for all material properties except

c_{110}	139 GPa	g_{110}	$6.46 \cdot 10^{-9}$ C ² /Nm ²
c_{120}	74 GPa	p_{110}	$-2.5 \cdot 10^{-5}$ C/m ² K
c_{220}	115 GPa	α_{10}	$7.41 \cdot 10^{-6}$ 1/K
e_{110}	15.1 C/m ²	α_{20}	$2.11 \cdot 10^{-6}$ 1/K
e_{120}	-5.2 C/m ²	ρ_0	7500 kg/m ³

Table 1. Mechanical and electrical properties for PZT_4.

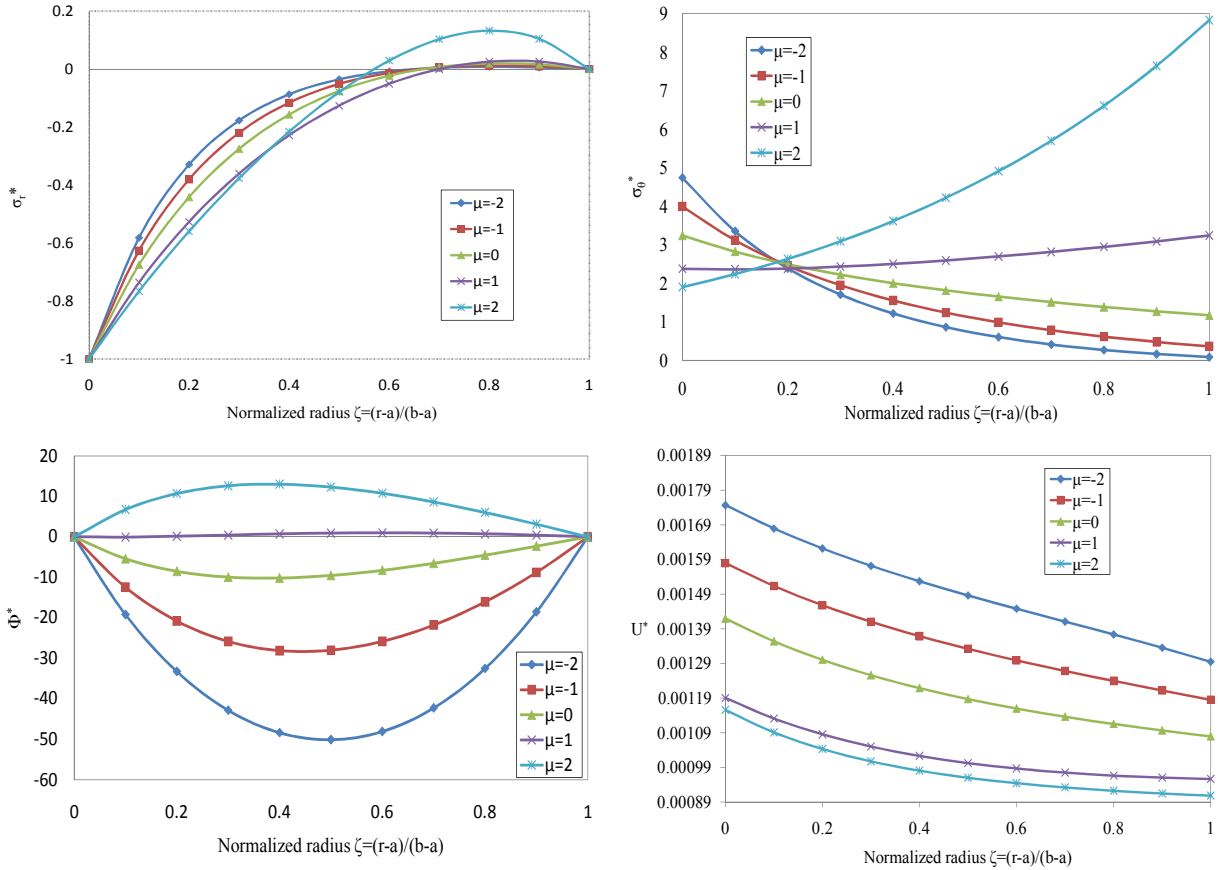


Figure 3. Case 1: Distribution of (normalized) radial stress σ_r^* , circumferential stress σ_θ^* , electric potential Φ^* , and radial displacement U^* for different values of μ .

for $\mu = 1$. Furthermore, this figure shows that the hoop stresses are increasing at the outer surface and decreasing at the inner surface with increasing the material inhomogeneity exponent μ .

Although for the first case no electric potential is imposed however an induced electric potential distribution satisfying the zero potential boundary condition is obtained in which the minimum potential distribution belongs to the material identified by $\mu = -2$ and the maximum distribution belongs to $\mu = 2$. It is concluded from Figure 3, bottom left, that the material inhomogeneity exponent μ significantly affects the induced electric potential.

The radial displacement distributions for different values of the inhomogeneity material μ are demonstrated in Figure 3, bottom right. It is seen from this figure that the radial displacement decreases with increasing μ and its maximum value is located at the inner radius of the cylinder.

Case 2. Figures 4 show the results of case 2, in which purely electric potential is imposed. The tensile radial and hoop stresses are induced in the thickness of the cylinder. The top two graphs of Figure 4 show that the material inhomogeneity exponent significantly affect the induced stresses throughout the thickness. Radial induced stresses satisfy the free-free boundary conditions of the cylinder. Radial and

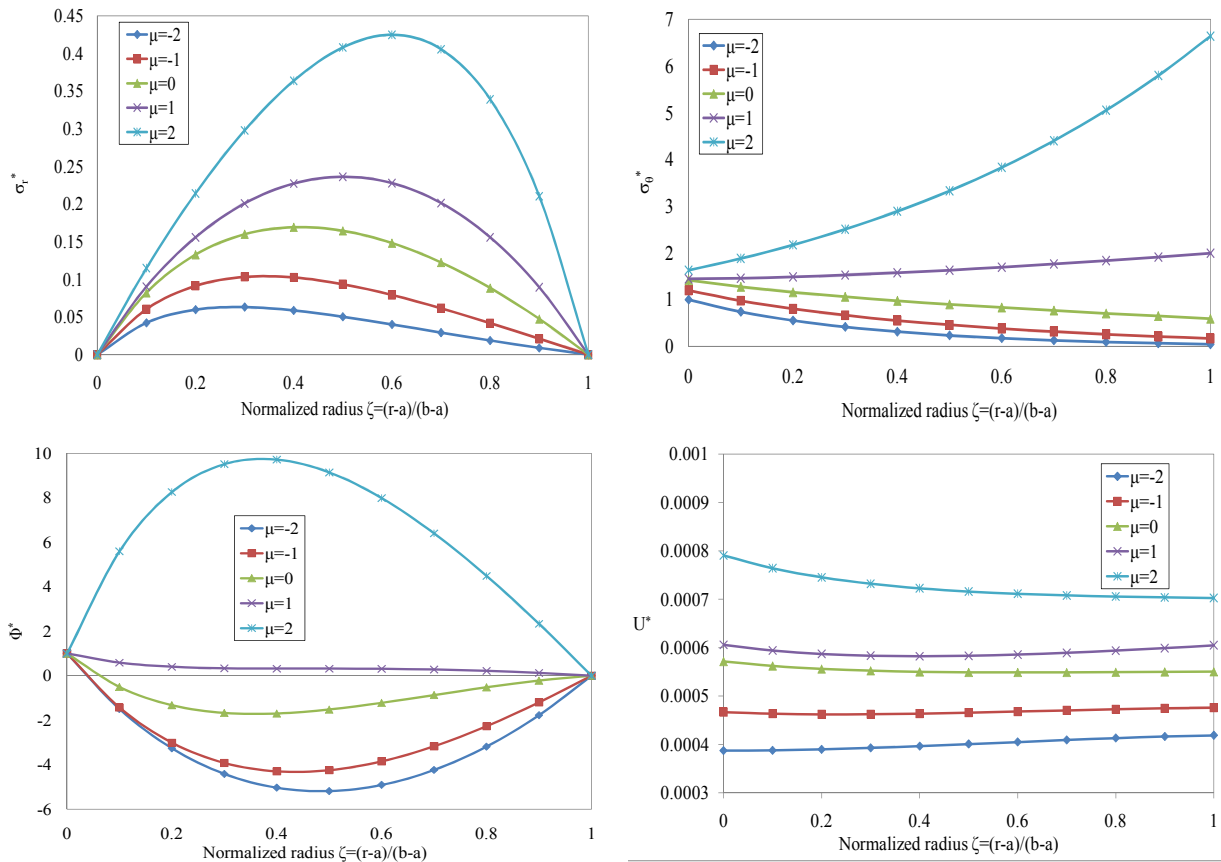


Figure 4. Case 2: Distribution of (normalized) radial stress σ_r^* , circumferential stress σ_θ^* , electric potential Φ^* , and radial displacement U^* for different values of μ .

hoop induced stresses increase when the exponent μ rises. It is clear from Figure 4, top right, that for nonpositive values of the index μ , the hoop stresses are decreased and for positive values of the index μ , the hoop stresses are increased throughout the thickness.

The electric potential distributions satisfy the boundary conditions of this case is shown in Figure 4, bottom left. The electric potential distribution is significantly affected by the material exponent μ so that for positive values of μ is positive throughout the thickness and for negative values of μ is almost negative throughout the thickness. The minimum electric potential belongs to material identified by $\mu = -2$ and the maximum electric potential belongs to $\mu = 2$.

Variation of displacement along radius is shown in Figure 4, bottom right. It is almost a uniform distribution throughout the thickness however its value is affected by the material exponent μ so that as μ increases displacement also increases.

Case 3. In case 3 (Figure 5), the EGPM rotating hollow cylinder is subjected to an external uniform pressure, zero electric potential difference between the inner and outer surfaces and free mechanical boundary condition at the inner surface. The compressive radial stresses for different values of μ are

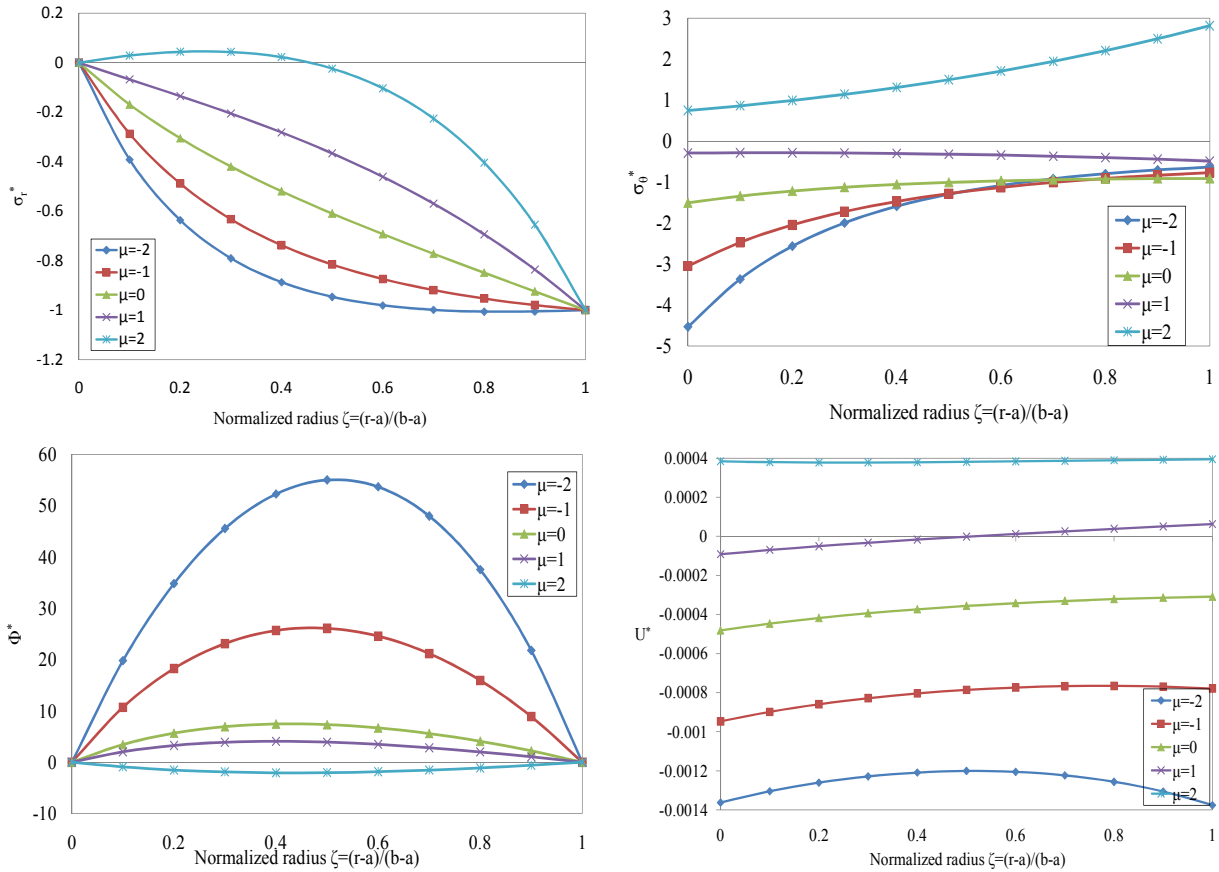


Figure 5. Case 3: Distribution of (normalized) radial stress σ_r^* , circumferential stress σ_θ^* , electric potential Φ^* , and radial displacement U^* for different values of μ .

shown in Figure 5, top left. It is clear that the radial stresses satisfy the boundary conditions. The material inhomogeneity exponent μ significantly affects the radial stresses throughout the thickness. It is also obvious from this figure that the radial stress increases with increasing exponent μ . The hoop stresses are illustrated in Figure 5, top right. Hoop stresses are increasing by increasing the exponent μ . However except for the exponent $\mu = 2$ the hoop stresses approaches almost the same value at the outer surface of the cylinder.

Although for this case no electric potential is imposed however an electric potential distribution satisfying the zero potential boundary condition is induced in which the minimum potential distribution belongs to the material identified by $\mu = 2$ and the maximum distribution belongs to $\mu = -2$. It is concluded from Figure 5, bottom-a left, that the material inhomogeneity exponent μ significantly affects the induced electric potential. Comparing the induced electric potential in this case with the case in which the cylinder is subjected to an internal pressure a fully reverse potential distribution can be identified.

Variation of displacement along radius is shown in Figure 5, bottom right. It is almost a uniform distribution throughout the thickness however its absolute value is affected by the material exponent μ so that as μ increases the absolute value of displacement decreases.

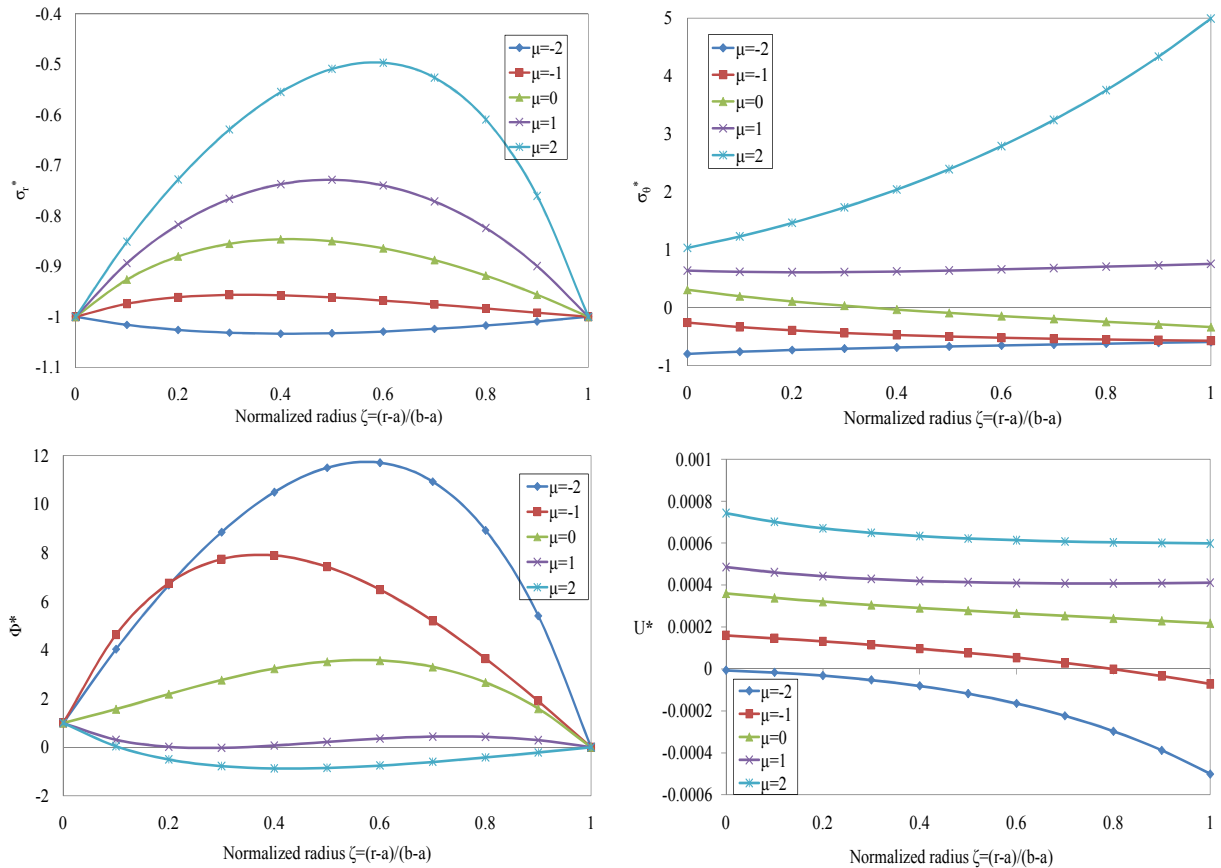


Figure 6. Case 4: Distribution of (normalized) radial stress σ_r^* , circumferential stress σ_θ^* , electric potential Φ^* , and radial displacement U^* for different values of μ .

Case 4. In case 4 (Figure 6) superposition of cases 1, 2 and 3 is investigated. Distribution of radial and hoop stresses along the radius for different values of exponent μ are shown in the top two graphs for Figure 6. It is obvious from these figures that the inhomogeneity parameter μ has a major effect on the electrothermoelastic stresses. Electric potential and radial displacement distributions in the bottom two graphs of Figure 6 are indeed superposition of previous cases 1, 2 and 3.

6. Conclusions

Using the hypergeometric function, closed form solution for EGP rotating hollow cylinder, is presented with four different sets of boundary conditions. The analytical solution of homogeneous piezoelectric rotating hollow cylinder is fully covered by setting the material inhomogeneity $\mu = 0$, our results for the homogeneous PZT_4 hollow cylinder are almost the same as those in [Galic and Horgan 2003]. The correctness of the present solution is then verified in this respect.

It is concluded from the present result that the inhomogeneity exponent μ significantly affects the radial and hoop stress distributions. This implies that the electrothermomechanical fields in EGP cylindrical

structures can be optimized for specific applications by selecting a suitable inhomogeneity parameter. Moreover, the inhomogeneous constants presented in the present study are useful parameters from a design point of view in that they can be tailored for special applications to control the distributions of electrothermoelastic stresses.

The technological implications of this study are significant, e.g., the amount of hoop stress resulting from thermomechanical loads in an EGPM rotating hollow cylinder can be reduced or neutralized by a suitably applied electric potential field and material inhomogeneity. Henceforward, our results can help engineers to design a rotating piezoelectric pressure vessel made of EGPM with an optimum distribution of stresses.

List of symbols

a, b	Inner and outer radius [m]	C_{ij} ($i, j = 1, 2$)	Elastic constant [N/m ²]
r	Radial variable [m]	e_{1i} ($i = 1, 2$)	Piezoelectric coefficient [C/m ²]
u_r	Radial displacement [m]	g_{11}	Dielectric constant [C ² /Nm ²]
β, μ	Inhomogeneity parameters	p_{11}	Pyroelectric coefficient [C/m ² K]
σ_θ, σ_r	Components of stresses [N/m ²]	φ	Electric potential [W/A]
α_1, α_2	Thermal expansion coefficients [1/K]	D_r	Radial electric displacement [C/m ²]
λ_1, λ_2	Thermal modulus [N/m ² K]	ω	Angular velocity [rad/s]
$T(r)$	Temperature distribution [K]	ρ	Mass density [kg/m ³]
h	Ratio of the convective heat-transfer coefficient [W/K]		
k	Thermal conduction coefficient [W/mK]		

Nondimensional quantities:

$$T^* = \frac{T(r)}{T_0}, \quad \zeta = \frac{r-a}{b-a}, \quad \sigma_i^* = \frac{\sigma_i}{P_a} (i = r, \theta), \quad U^* = \frac{u(r)}{a}, \quad \Phi^* = \frac{\phi}{\phi_a}$$

Acknowledgment

The authors thank the referees for their valuable comments.

References

- [Abramowitz and Stegun 1965] M. Abramowitz and I. A. Stegun (editors), *Handbook of Mathematical Functions*, Dover, New York, 1965.
- [Babaei and Chen 2008] M. Babaei and Z. Chen, "Analytical solution for the electromechanical behavior of a rotating functionally graded piezoelectric hollow shaft", *Arch. Appl. Mech.* **78** (2008), 489–500.
- [Brischetto and Carrera 2009] S. Brischetto and E. Carrera, "Refined 2D models for the analysis of functionally graded piezoelectric plates", *J. Intelligent Mater. Syst. Struct.* **20**:15 (2009), 1783–1797.
- [Chen and Shi 2005] Y. Chen and Z.-f. Shi, "Analysis of a functionally graded piezothermoelastic hollow cylinder", *J. Zhejiang Univ. Sci. A* **6** (2005), 956–961.
- [Dai et al. 2010] H.-L. Dai, L. Hong, Y.-M. Fu, and X. Xiao, "Analytical solution for electromagnetothermoelastic behaviors of a functionally graded piezoelectric hollow cylinder", *Appl. Math. Model.* **34**:2 (2010), 343 – 357.
- [Fung 1965] Y. C. Fung, *Foundations of solid mechanics*, Prentice-Hall, New York, 1965.
- [Galic and Horgan 2002] D. Galic and C. Horgan, "Internally pressurized radially polarized piezoelectric cylinders", *J. Elasticity* **66** (2002), 257–272.

- [Galic and Horgan 2003] D. Galic and C. O. Horgan, “The Stress Response of Radially Polarized Rotating Piezoelectric Cylinders”, *J. Appl. Mech. (ASME)* **70**:3 (2003), 426–435.
- [Ghorbanpour et al. 2006] A. Ghorbanpour, S. Golabi, and M. Saadatfar, “Stress and electric potential fields in piezoelectric smart spheres”, *J. Mech. Sci. Tech. (Korea)* **20** (2006), 1920–1933.
- [Hosseini et al. 2007] S. Hosseini, M. Akhlaghi, and M. Shakeri, “Transient heat conduction in functionally graded thick hollow cylinders by analytical method”, *Heat and Mass Transfer* **43** (2007), 669–675.
- [Khoshgoftar et al. 2009] M. J. Khoshgoftar, A. G. Arani, and M. Arefi, “Thermoelastic analysis of a thick walled cylinder made of functionally graded piezoelectric material”, *Smart Mater. Struct.* **18**:11 (2009), 115007.
- [Li et al. 2010] X.-F. Li, X.-L. Peng, and K. Y. Lee, “Radially polarized functionally graded piezoelectric hollow cylinders as sensors and actuators”, *Eur. J. Mech. A Solids* **29**:4 (2010), 704 – 713.
- [Lu et al. 2005] P. Lu, H. Lee, and C. Lu, “An exact solution for functionally graded piezoelectric laminates in cylindrical bending”, *Int. J. Mech. Sci.* **47**:3 (2005), 437 – 458.
- [Lu et al. 2006] P. Lu, H. Lee, and C. Lu, “Exact solutions for simply supported functionally graded piezoelectric laminates by Stroh-like formalism”, *Compos. Struct.* **72**:3 (2006), 352 – 363.
- [Pan and Han 2005] E. Pan and F. Han, “Exact solution for functionally graded and layered magneto-electro-elastic plates”, *Int. J. Eng. Sci.* **43**:3-4 (2005), 321 – 339.
- [Saadatfar and Razavi 2009] M. Saadatfar and A. Razavi, “Piezoelectric hollow cylinder with thermal gradient”, *J. Mech. Sci. Tech. (Korea)* **23** (2009), 45–53.
- [Tiersten 1969] H. F. Tiersten, *Linear piezoelectric plate vibrations*, Plenum Press, New York, 1969.
- [Zhong and Shang 2003] Z. Zhong and E. T. Shang, “Three-dimensional exact analysis of a simply supported functionally gradient piezoelectric plate”, *Int. J. Solids Struct.* **40**:20 (2003), 5335 – 5352.

Received 2 Jul 2010. Revised 22 Sep 2010. Accepted 27 Sep 2010.

ALI GHORBANPOUR ARANI: aghorban@kashanu.ac.ir

Mechanical Engineering Department, University of Kashan, Kilometre 6 Bolvar Ghotb Ravandi, POBox 87317-51167, Kashan, Iran

ABBAS LOGHMAN: aloghman@kashanu.ac.ir

Mechanical Engineering Department, University of Kashan, Kilometre 6 Bolvar Ghotb Ravandi, POBox 87317-51167, Kashan, Iran

ALI ABDOLLAHITAHERI: abdollahitaheri@grad.kashanu.ac.ir

Mechanical Engineering Department, University of Kashan, Kilometre 6 Bolvar Ghotb Ravandi, POBox 87317-51167, Kashan, Iran

VAHID ATABAKHSHIAN: v.atabakhshian@gmail.com

Mechanical Engineering Department, University of Kashan, Kilometre 6 Bolvar Ghotb Ravandi, POBox 87317-51167, Kashan, Iran

JOURNAL OF MECHANICS OF MATERIALS AND STRUCTURES

jomms.org

Founded by Charles R. Steele and Marie-Louise Steele

EDITORS

CHARLES R. STEELE Stanford University, USA
DAVIDE BIGONI University of Trento, Italy
IWONA JASIUK University of Illinois at Urbana-Champaign, USA
YASUhide SHINDO Tohoku University, Japan

EDITORIAL BOARD

H. D. BUI École Polytechnique, France
J. P. CARTER University of Sydney, Australia
R. M. CHRISTENSEN Stanford University, USA
G. M. L. GLADWELL University of Waterloo, Canada
D. H. HODGES Georgia Institute of Technology, USA
J. HUTCHINSON Harvard University, USA
C. HWU National Cheng Kung University, Taiwan
B. L. KARIHALOO University of Wales, UK
Y. Y. KIM Seoul National University, Republic of Korea
Z. MROZ Academy of Science, Poland
D. PAMPLONA Universidade Católica do Rio de Janeiro, Brazil
M. B. RUBIN Technion, Haifa, Israel
A. N. SHUPIKOV Ukrainian Academy of Sciences, Ukraine
T. TARNAI University Budapest, Hungary
F. Y. M. WAN University of California, Irvine, USA
P. WRIGGERS Universität Hannover, Germany
W. YANG Tsinghua University, China
F. ZIEGLER Technische Universität Wien, Austria

PRODUCTION contact@msp.org

SILVIO LEVY Scientific Editor

Cover design: Alex Scorpan

Cover photo: Ev Shafir

See <http://jomms.org> for submission guidelines.

JoMMS (ISSN 1559-3959) is published in 10 issues a year. The subscription price for 2011 is US \$520/year for the electronic version, and \$690/year (+\$60 shipping outside the US) for print and electronic. Subscriptions, requests for back issues, and changes of address should be sent to Mathematical Sciences Publishers, Department of Mathematics, University of California, Berkeley, CA 94720–3840.

JoMMS peer-review and production is managed by EditFLOW™ from Mathematical Sciences Publishers.

PUBLISHED BY
 **mathematical sciences publishers**
<http://msp.org/>

A NON-PROFIT CORPORATION

Typeset in L^AT_EX

Copyright ©2011 by Mathematical Sciences Publishers

Journal of Mechanics of Materials and Structures

Volume 6, No. 6

July–August 2011

- Modelling of acoustodiffusive surface waves in piezoelectric-semiconductor composite structures** J. N. SHARMA, K. K. SHARMA and A. KUMAR 791
- Dynamic fracture tests of polymethylmethacrylate using a semicircular bend technique** S. HUANG, S.-N. LUO, B. S. A. TATONE and K. XIA 813
- Stress and buckling analyses of laminates with a cutout using a {3, 0}-plate theory** ATILA BARUT, ERDOGAN MADENCI and MICHAEL P. NEMETH 827
- Electrothermomechanical behavior of a radially polarized rotating functionally graded piezoelectric cylinder** A. G. ARANI, A. LOGHMAN, A. ABDOLLAHITAHERI and V. ATABAKHSHIAN 869
- Large-amplitude dynamic analysis of stiffened plates with free edges** ANIRBAN MITRA, PRASANTA SAHOO and KASHINATH SAHA 883
- Dynamic behavior of magnetostrictive/piezoelectric laminate cylindrical shells due to electromagnetic force** B. BIJU, N. GANESAN and K. SHANKAR 915
- Geometrically nonlinear thermomechanical response of circular sandwich plates with a compliant core** YEOSHUA FROSTIG and OLE THOMSEN 925



1559-3959(2011)6:6;1-A